Metal-to-insulator transition in $LaAl_{1-x}Cr_xO_3/SrTiO_3$ oxide heterostructures guided by electronic reconstruction

Pramod Kumar,[1] Prabir Pal,[2] A. K. Shukla,[2] J. J. Pulikkotil,[1,2] and Anjana Dogra[1,2]

[1]*Academy of Scientific and Innovative Research (AcSIR), CSIR-National Physical Laboratory (CSIR-NPL) Campus, Dr. K. S. Krishnan Road, New Delhi - 110012, India*

[2]*CSIR-National Physical Laboratory, Dr. K. S. Krishnan Road, New Delhi - 110012, India*

(Received 22 September 2014; revised manuscript received 22 February 2015; published 13 March 2015)

Despite continuous efforts, a conceptual perception on the origin of quasi-two-dimensional electron gas (q-2DEG) in oxide heterostructures remains far from any generalization. Along this perspective, a systematic study identifying systems that exhibit heterointerface conductivity ($LaAlO_3/SrTiO_3$) and that do not ($LaCrO_3/SrTiO_3$) is undertaken. High quality $LaAl_{1-x}Cr_xO_3$ ($0 \leqslant x \leqslant 1$) films were fabricated on TiO_2 terminated $SrTiO_3$ (001) substrates using a pulsed laser deposition technique and its growth was monitored by reflection high energy electron diffraction (RHEED). The transport and photoemission spectroscopy experiments reveal that the the origin of heterointerface q-2DEG is associated with Ti^{3+} states and that it ceases to exist with increasing Cr ion concentration in the overlayer films. Following experimental evidences of the Cr concentration dependent metal-insulator electronic phase transition at the heterointerface, explanation is sought within the realms of a polar catastrophe model. Based on our transport and spectroscopy measurements, we propose that an electronic reconstruction drives the formation of q-2DEG for pristine LAO/STO and Al rich samples due to the formation of Ti^{3+}/Ti^{4+} mixed valent state, while for heavily doped Cr samples, the required electron count necessary to solve the polar catastrophe instability are trapped in the $LaAl_{1-x}Cr_xO_3$ overlayers in the Cr 3*d* states. These trapped electrons in the overlayers are manifested in the form of Cr^{2+} ions.

DOI: 10.1103/PhysRevB.91.115127 PACS number(s): 68.37.Xy, 68.35.Ct, 73.40.−c, 71.30.+h

I. INTRODUCTION

The origin of quasi-two-dimensional electron gas (q-2DEG) at the interface of insulating oxides [1], such as $LaAlO_3/SrTiO_3$ (LAO/STO), is associated with both extrinsic and intrinsic factors. Variance in the q-2DEG properties with change in synthesis conditions infer to extrinsic factors such as O_2 defects [2–4] and intersite cation mixing [5–9]. On parallel grounds, modeling the oxide heterointerface as a polar-nonpolar interface leads to the manifestation of the polar catastrophe scenario [10], which being intrinsic in origin develops a diverging potential, in proportion with increasing LAO film thickness. In this model, polarity compensation occurs via charge transfer across the LAO film to the TiO_2 terminated substrate. Exigencies to the charge neutrality condition therefore switches on the intrinsic chemical property of the interface transition metals (Ti ions) to adjust their valence state, resulting in the formation of q-2DEG at the interface via the Ti^{3+} states [11–13].

Although both models appear legitimate, a general picture of the origin of q-2DEG in oxide heterointerfaces is still lacking. Recent spectroscopy measurements find that the defect states resulting from O_2 vacancies lie in the midgap energy range and are rather very localized, resulting in no significant contribution to the interface conductivity [14,15]. However, the origin of these in-gap states has also been attributed to strong O 2*p*-Ti 3*d* hybridization [16,17] similar to the mechanism as proposed in Ref. [18] for impurities in semiconductors and also due to the formation of a two-dimensional polaronic phase related to a strong electron-lattice interaction [19]. On the other hand, the high energies involved in the synthesis trigger a possibility of alloying, whereby cations from the film and substrate mutually swap their ionic positions imparting chemical disorder at the interface [5,20]. A confined disorder of La/Sr (and Al/Ti), La/Al non-stoichiometry would also induce conductivity [5,21–24]. However, a couple of facts forbid intersite chemical disorder to be regarded as a universal mechanism of q-2DEG at heterointerfaces. For example, in case of LAO/STO, the critical thickness to exhibit q-2DEG is found to be 4 unit cell (u.c.) [11,25–29], and the depth of the q-2DEG into the STO substrate has been estimated to be 70 Å ($\simeq$17−20 u.c.) [13,30,31]. If the origin of q-2DEG is associated with La/Sr disorder due to intermixing, La ions would diffuse over larger spatial lengths into the substrate. This would enforce a proportionate migration of Sr ions to 4 u.c. LAO film overlayers, implying large chemical inhomogeneity across the interface. Such a chemical inhomogeneity across the interface has not been observed, so far.

Besides, La/Sr disorder inducing q-2DEG in LAO/STO and not in $LaCrO_3/SrTiO_3$ (LCO/STO) is also worth mentioning. If cation intermixing of Sr and La drives in q-2DEG, then it could be well presumed that any La based perovskite, grown epitaxially on TiO_2 terminated STO substrate, would exhibit a conducting heterointerface. It may be noted that identical synthesis conditions suffice layer-by-layer growth of both LAO and LCO films on TiO_2 terminated STO. So extrinsic factors governing only La/Sr intersite mixing in LAO/STO and that both La/Sr and Cr/Ti inter-site mixing in equal proportions in LCO/STO seem to be less satisfactory [20,32]. The question then to be addressed is whether there exists any universal mechanism which can explain the conducting (insulating) heterointerface of LAO/STO (LCO/STO) on equal footing. To systematically address this view, we have synthesized and characterized the properties of $LaAl_{1-x}Cr_xO_3$ films on TiO_2 terminated $SrTiO_3$ substrate, under similar growth conditions, given that at its concentration extrema $x = 0$ and 1, the heterointerface is conducting and insulating,

respectively. In this work, with the help of transport and photoemission spectroscopy measurements performed on high quality $LaAl_{1-x}Cr_xO_3/SrTiO_3$ heterointerfaces, we argue that electronic reconstruction can be considered as a universal model for q-2DEG formation in oxide heterostructures. Based on our experimental findings, we propose that an electronic reconstruction drives the formation of q-2DEG for LAO/STO and Al rich samples ($0 \leqslant x \leqslant 0.4$) due to the formation of Ti^{3+}/Ti^{4+} mixed valent state, while for heavily doped ($x \geqslant 0.6$) Cr samples, the threshold electron count necessary to solve the polar catastrophe instability are trapped in the $LaAl_{1-x}Cr_xO_3$ overlayers in the Cr 3*d* states. These trapped electrons in the overlayers manifest in the form of Cr^{2+} state.

II. EXPERIMENTAL DETAILS

A. Growth and transport measurements

Six u.c. ($\simeq$24 Å) thick samples of $LaAl_{1-x}Cr_xO_3$ ($0 \leqslant x \leqslant 1$) (LACO) were fabricated on the TiO_2 terminated STO (001) single crystal substrates using a pulsed laser deposition (PLD) technique. STO (001) substrates were pretreated with the standard buffer hydrofluoric (NH_4F-HF) solution for 30 s to achieve uniform TiO_2 termination. After this treatment, the substrate was annealed for about 1.5 h at 830 °C in the oxygen pressure of 7.4×10^{-2} mbar before commencing the deposition. Thereafter, deposition for each of the composition was performed at 800 °C with oxygen partial pressure of 1×10^{-4} mbar. Deposition was performed using a KrF laser ($\lambda = 248$ nm) with the repetition rate of 1 Hz and energy density in the range of 0.50–0.62 J cm^{-2}. *In situ* reflection high energy electron diffraction (RHEED) has been used to monitor the growth mode and thickness of films. After deposition, the samples were cooled down to room temperature in a similar O_2 partial pressure in order to minimize the formation of oxygen vacancies, if any. Sheet resistance and Hall measurements of the interfaces were performed using a four-probe Van der Pauw method in a Quantum Design magnetic property measurements system (MPMS) which gives access to 7 T magnetic field in the temperature range from 300 to 2 K. Stable, low resistivity contacts with the q-2DEG were made by wire bonding using thin Al wires. In order to probe the LACO/STO interface directly using photoemission spectroscopy we have restricted our growth to 6 u.c., knowing the fact that the optimized thickness to observe the q-2DEG in the LAO/STO system is 4 u.c.

B. Photoemission spectroscopy

Photoemission spectroscopy (PES) measurements were performed using an ultrahigh vacuum (UHV) Omicron multiprobe surface analysis system (MPSAS) equipped with a monochromatic Al $K\alpha$ x-ray source for x-ray photoelectron spectroscopy (XPS), gas discharge lamp (He I = 21.2 eV) for ultra-violet photoelectron spectroscopy (UPS) and a seven channeltron hemispherical electron energy analyzer (EA 125). Base pressure of the experimental chamber was 4.0×10^{-11} Torr. All the samples were mounted on the sample plates using spot welded Ta foils. An electrical contact was established between the sample surface and grounded sample plate with a highly conducting UHV compatible Ag paint in order to avoid charging during the PES measurements due to the insulating nature of samples. This procedure helped us to avoid any significant time dependent charging. However, finite charging was still observed and it was corrected using C 1*s* (284.6 eV) core-level binding energy (BE). C 1*s* core levels were measured throughout the experiment particularly before and after each XPS spectra to correct any small shift due to charging. All binding energies were referenced to the Fermi level (E_F) position of Au film in electrical contact with the sample and were cross checked using the Fermi edge of clean polycrystalline Ag foil. All the spectra reported here were obtained at an emission angle of 40° while UPS spectra were recorded in normal emission using He-I radiation at room temperature. Total energy resolution, estimated from the width of the Fermi edge of a polycrystalline Ag sample, was about 450 meV for XPS (monochromatic Al $K\alpha$) and 100 meV for UPS. All the samples were transferred *ex situ* to the PES experimental chamber after growth in a separate PLD chamber. Before PES measurements, each sample has been annealed in UHV. The temperature was raised to 350 °C very slowly and then kept at this temperature for 10 h. In all the cases, the base pressure inside the chamber during annealing treatment was better than 1.0×10^{-9} Torr. Reduction of surface adsorbed feature in the O 1*s*, C 1*s* peak area and well defined multiplet structure of La 3*d* and 4*d* spectra confirm the relatively clean surfaces of all samples after this annealing treatment. More details of effect of annealing temperature are given in Appendix A. A Shirley background has been subtracted from the raw data.

III. RESULTS

A. Growth and structural characterization

The RHEED specular beam intensity oscillations as a function of growth time (or u.c.), for series of ultrathin films of 6 u.c. of LACO/STO for ($0 \leqslant x \leqslant 1$) are shown in Fig. 1. Growth control with the precision of single u.c. is evident from the observed *in situ* RHEED oscillations which assures not only the good quality interfaces but also reflects a clean

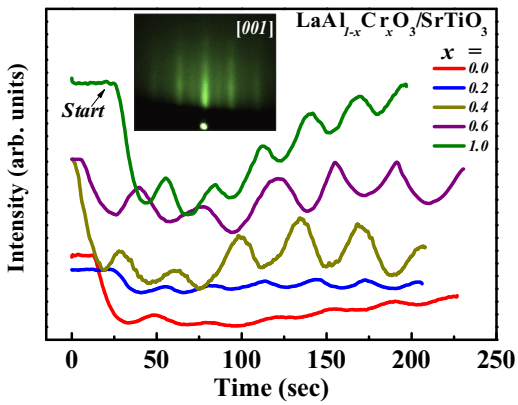

FIG. 1. (Color online) Observed RHEED intensity oscillations along the (001) crystallographic direction during the growth of $LaAl_{1-x}Cr_xO_3$ (LACO) ($0 \leqslant x \leqslant 1$) film overlayers on TiO_2 terminated $SrTiO_3$. Inset shows a clean streaky RHEED pattern for LAO/STO. A similar streaky pattern was observed for all the samples in LACO/STO series.

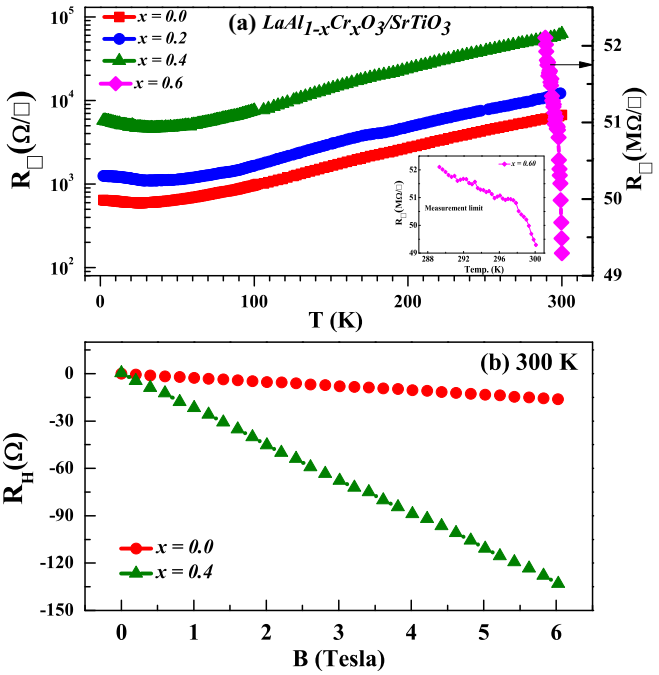

FIG. 2. (Color online) (a) Temperature dependence of sheet resistance for 6 u.c. $LaAl_{1-x}Cr_xO_3$ ($0 \leqslant x \leqslant 0.6$) films on TiO_2 terminated $SrTiO_3$ (001) substrate from 300 to 2 K, indicating a metallic behavior for $0 \leqslant x \leqslant 0.4$ and an insulating behavior for $x = 0.6$. The inset shows temperature dependence of sheet resistance for the $x = 0.6$ sample. (b) Hall resistance at 300 K for $x = 0.0$ and 0.4. The sheet carrier density is 2.35×10^{14} and 2.83×10^{13} cm^{-2} for $x = 0$ and $x = 0.4$ samples, respectively.

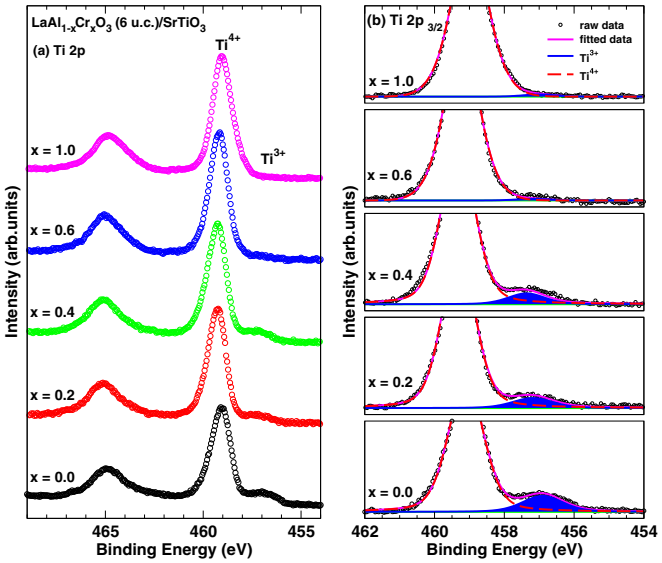

FIG. 3. (Color online) (a) Ti $2p$ core-level photoemission spectra of the $LaAl_{1-x}Cr_xO_3/SrTiO_3$, ($0 \leqslant x \leqslant 1$). All the spectra have been normalized at 454 eV and shifted along the y axis for clarity. (b) Ti $2p_{3/2}$ core-level photoemission spectra for different Cr concentration (x). Experimental spectra (open circles), fitted spectra (magenta solid line), deconvoluted components used to fit Ti^{4+} (red dashed line), and Ti^{3+} (blue shaded) are also shown. Shirley background subtraction has been used for all the spectra. Main peak (Ti^{4+}) has been truncated in height to present the Ti^{3+} related peak clearly.

layer by layer u.c. growth. The inset of Fig. 1 shows the RHEED pattern observed for 6 u.c. LAO/STO along the (001) crystallographic direction. The observed streaky pattern throughout the growth process confirms the smooth, 2D, and epitaxial surface for all the films deposited on TiO_2 terminated STO substrate. Intermediate streaks with feeble intensity may infer to a $(1 \times 2)/(2 \times 1)$ reconstructed surface.

B. Electronic transport

Figure 2(a) shows the variation of sheet resistance ($R_\square$) of LACO/STO as a function of temperature (T) over the range $2 \leqslant T \leqslant 300$ K. Consistent with the earlier reports, LAO/STO ($x = 0$) displays metallic behavior with its sheet resistance decreasing with decreasing T. With increasing x, the metallic characteristics diminish as evidenced by the increasing sheet resistance. For example, at $T = 300$ K (2 K), the sheet resistance for $x = 0$, 0.2, and 0.4 are 6.73 (0.64), 12.15 (1.25), and 62.59 (5.72) kΩ/□, respectively. The sheet resistance at 300 K for $x = 0.6$ heterostructure is very high (>1 MΩ) which is indicative of an insulating heterointerface.

The Hall measurements were performed at room temperature for $x = 0.0$ and 0.4. The sheet carrier density (n_s) is calculated from the slope of Hall resistance $R_H = B/n_s e$ shown in Fig. 2(b). The extracted sheet carrier density from the Hall measurements for $x = 0$ is 2.35×10^{14} cm^{-2} while the $x = 0.4$ sample shows a decrease in the carrier density to 2.83×10^{13} cm^{-2}. The measured negative Hall resistance is indicative of the transport being dominated by the electrons. The Hall mobility at 300 K is 3.95 and 3.52 cm^2/V s for $x = 0$ and 0.4 samples, respectively. The observation of Cr concentration dependent metal-insulator transition and the substantial decrease in the carrier density are complementary. The observed trend clearly evidences to the fact that increasing Cr concentration in the LACO film overlayers suppress the heterointerface q-2DEG. We have also performed transport measurements on the samples which were subjected to the XPS measurements. Results are consistent with our earlier transport measurements of as-grown samples with an insignificant change in the sheet resistance.

C. Electronic structure

1. *Core-level spectra*

To understand the evolution of the electronic structure of the 6 u.c. LACO/STO system as a function of increasing Cr concentration, we have investigated the Ti $2p$ and Cr $2p$ core-level spectra, which are shown in Figs. 3(a) and 4(a), respectively. For LACO/STO, the Ti $2p_{3/2}$ and $2p_{1/2}$ spin-orbit doublet peaks are located at 459.1 and 464.8 eV BE, respectively. The Cr $2p_{3/2}$ and $2p_{1/2}$ spin-orbit doublet peaks are centered at 576.8 and 587.0 eV BE, respectively. These features remain invariant, irrespective of the overlayer film composition.

Closer view of the Ti $2p_{3/2}$ spectrum shows that it has two components—a main peak which is characteristic of the Ti^{4+} state emanating from the bulk substrate and the other component manifested as a shoulder to the lower binding

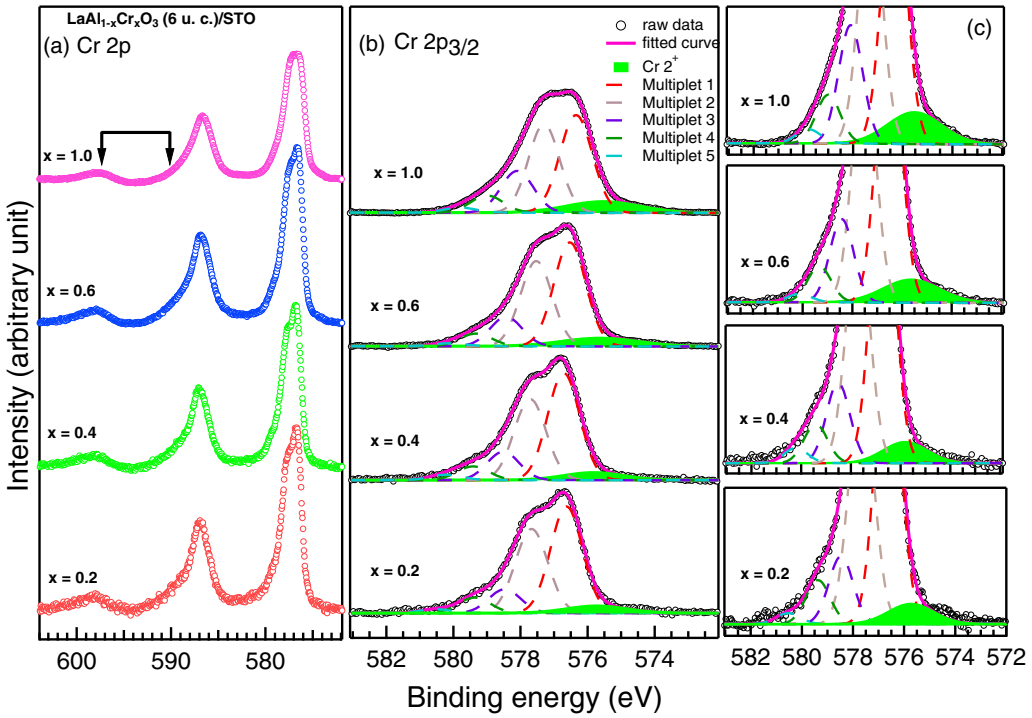

FIG. 4. (Color online) Cr $2p$ core-level photoemission spectra for the samples having different Cr concentration (x). Shakeup satellites are shown by arrows. All the spectra have been normalized at 572 eV binding energy and shifted along the y axis for clarity. (b) Cr $2p_{3/2}$ core-level photoemission spectra (open circles) for the samples having different Cr concentrations. Fitted spectra (thick solid line) and five multiplet components (dashed lines) used to fit each core level are also shown. Feature belonging to Cr^{2+} is shown as a shaded part. Each set of spectra have been normalized by the peak height of the highest peak and staggered along the y axis for clarity of presentation. (c) Main peak (Cr^{3+}) is truncated in height to present the Cr^{2+} related feature more clearly.

energy of the Ti^{4+} peak. The latter feature is unambiguously related to Ti^{3+} states, the origin of which can be associated with both intrinsic and extrinsic mechanisms of q-2DEG heterointerface conductivity [13,14,33–36]. We note that no prominent Ti^{3+} states were observed for bare TiO_2 terminated STO surface [37]. For $0 \leqslant x \leqslant 0.4$, the characteristics of the Ti^{3+} feature is well preserved, beyond which as x increases, the feature disappears.

To derive an estimate of Ti^{3+} as a function of x, we adopt to the χ^2 iterative fit of the Ti $2p_{3/2}$ core-level peak using two components corresponding to the Ti^{3+} and Ti^{4+} as shown in Fig. 3(b). Except for the peak integral and energy positions, the line shapes, widths (FWHMs), and all other parameters were assumed as invariants for the fitting of all core levels. Results of the fit are shown in Table I and Fig. 3(b). Consistent with the earlier XPS reports, for LAO/STO the weak Ti^{3+} peak, shaded component in Fig. 3(b), was determined 2.2 eV lower in binding energy with respect to the Ti^{4+} peak centered at 459.1 eV [13,14,33–36]. The relative percentage (normalized peak area) of Ti^{3+} to Ti^{4+} is estimated as 12.3% for LAO/STO and 7.2% for $x = 0.2$. This ratio tends to zero for systems with $x \geqslant 0.6$. In conjunction with transport measurements, the decrease in the concentration of Ti^{3+} ions evidence to its role in q-2DEG formation at the heterointerface of these systems.

On the other hand, the Cr $2p$ core level for $x = 1$ resembles that emanating from a Cr^{3+} state [38–41]. We also note the

TABLE I. Fitting parameters for the Ti $2p_{3/2}$ core-level spectra shown in Fig. 3(b). The binding energy positions and FWHM of both the components are also listed. Relative percentage of Ti^{3+} is calculated from the ratio of the area under the Ti^{3+} peak and total peak area ($Ti^{4+} + Ti^{3+}$). Uncertainty in determining the BE position and FWHM is estimated to be ±0.1 eV. Uncertainty in determining Ti^{3+} content is estimated to be ±5% of the base value.

Sample	Ti^{3+}		Ti^{4+}		ΔBE	
(x)	BE position	FWHM	BE position	FWHM	(Ti^{4+}- Ti^{3+})	Relative % of Ti^{3+}
0.0	456.90	1.36	459.10	1.18	2.2	12.3
0.2	457.18	1.36	459.31	1.12	2.1	7.2
0.4	457.37	1.36	459.32	1.12	2.0	7.0
0.6	457.19	1.10	459.22	1.11	2.0	0.2
1.0	457.00	1.10	459.00	1.12	2.0	0.1

TABLE II. The fitting parameters for the Cr $2p_{3/2}$ core-level spectra shown in Fig. 4(b). The binding energy positions of Cr^{2+} and Cr^{3+} components are also listed, where for Cr^{3+} the value represents the average of the multiplet peaks 1 and 2. Relative percentage of Cr^{2+} is calculated from the ratio of the area under the Cr^{2+} peak and total peak area (Cr^{2+}+ Cr^{3+}). Uncertainty in determining the BE position and FWHM is estimated to be ±0.1. Uncertainty in determining Cr^{2+} content is estimated to be ±5% of the base value.

Sample	Cr^{3+}	Cr^{2+}	ΔBE	
(x)	BE position	BE position	(Cr^{3+}- Cr^{2+})	Relative % of Cr^{2+}
0.2	577.15	575.73	1.42	5.3
0.4	577.25	575.84	1.41	5.3
0.6	577.03	575.63	1.40	7.8
1.0	576.82	575.53	1.30	9.3

subtle change in the main peak intensity and it has been discussed in Appendix B. Features such as multiplet splitting due to $2p$-$3d$ exchange interaction (manifested as the splitting of main peak) [41–43], and the shakeup satellites were also observed in the spectra shown in Fig. 4(a) [40,41,44]. Biesinger *et al.* [42] have successfully fitted the Cr $2p_{3/2}$ core level of Cr_2O_3 (Cr^{3+}, d^3) using five multiplet peaks based on a simple Hartee-Fock model (please see Appendix B for more details). Knowing that in our case of LACO, Cr is mainly in the 3+ valence state (d^3), we have used the same approach to fit the Cr $2p_{3/2}$ spectra of LACO/STO. These fittings are shown in Fig. 4(b). We have used a χ^2 iterative program for fitting the Cr $2p_{3/2}$ spectra with five multiplet components (Gaussian) with separation of 1.0, 0.8, 0.9, and 0.8 eV (going from right to left of main peak) and FWHM of each component was 1.1 eV. Individual fitting components are shown as dashed lines in Fig. 4. Even though most part of the spectrum was successfully fitted using this approach, an extra component [shown as shaded region in Fig. 4(b)] was necessary to fit the tail of the spectrum at the lower binding energy side. This component had finite contribution for all LACO/STO heterostructures (except $x = 0$). The main peak position corresponding to Cr^{3+}, which can be represented by average position of first two dominant multiplet peaks, is estimated to be 576.8 eV. An extra component (shaded region) lies 1.3 eV below the main peak with FWHM of 2.5 eV and its energy separation from the main peak is close to the expected separation of Cr^{3+} and Cr^{2+} binding energies [45,46]. Therefore, we attribute this component to Cr^{2+}. Adopting to the same fitting routine for $0 \leqslant x \leqslant 1$, we have calculated the evolution of Cr^{2+} contribution to the spectra and it is shown in Table II, together with the fitting parameters. Summary of all the fitting parameters is provided in Table III in Appendix B. Colby *et al.* [32] have recently suggested the presence of Cr^{2+} in LCO/STO ($x = 1$) on the basis of electron energy loss spectroscopy (EELS) data. However, the authors also suggest a small but finite amount of Ti^{3+} in the overlayer LCO film side, which they attribute to cation intermixing. Contrary to their suggestion, our Ti $2p$ core-level analysis do not find any evidence of Ti^{3+} features for $0.6 \leqslant x \leqslant 1$ heterostructures.

Figure 5 shows the calculated percentages of Ti^{3+} (Table I) and Cr^{2+} (Table II) as a function of x. It is evident that

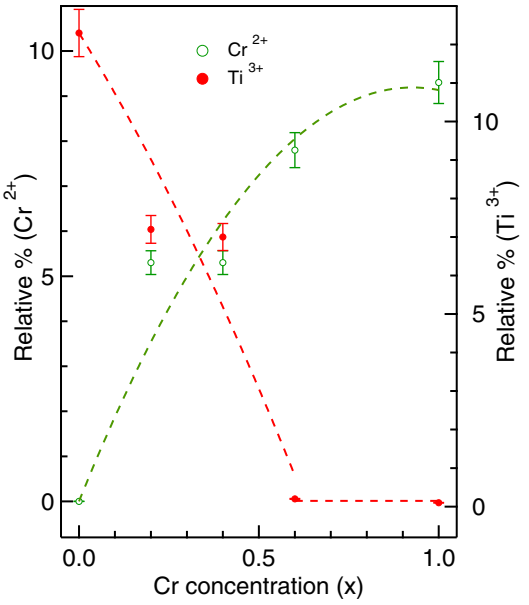

FIG. 5. (Color online) Relative percentage of Cr^{2+} (left axis) and Ti^{3+} (right axis) as a function of Cr concentration (x) in $LaAl_{1-x}Cr_xO_3/SrTiO_3$ ($0 \leqslant x \leqslant 1$) heterostructures. Dashed lines serve as a guide to the eye. Error bars representing experimental uncertainty (±5% of the base value) in quantification are also shown.

mixed valence states coexist over the entire LACO/STO phase diagram, with Ti^{3+}/Ti^{4+} and Cr^{2+}/Cr^{3+}. As being accepted that the heterointerface conductivity in LAO/STO is associated with Ti^{3+}, its steady decrease with increasing x in conjunction with decreasing conductivity as observed from the transport measurements, evidences to a direct correlation between the mixed valence states of Ti and Cr with the creation and annihilation of heterointerface q-2DEG state.

2. *Valence band spectra*

In order to study the evolution of valence band (VB) states in LACO/STO ($0 \leqslant x \leqslant 1$), we measured the XPS VB spectra as shown in Fig. 6(a). The top of the valence band for $0.2 \leqslant x \leqslant 1$ is mainly comprised of Cr $3d$ derived states, with a peak at 2.4 eV, with small admixture of O $2p$ states. The energy window between 3 and 8 eV is primarily dominated by O $2p$ states [20,41]. The overall shape of the VB for $x = 0$ and $x = 1$ is in agreement with earlier reports. We note that the binding energy position of Cr $3d$ and O $2p$ states are different compared to bulklike samples due to surface and interface effects. The inset of Fig. 6(a) illustrates a continuous increase in the relative intensity of the Cr $3d$ feature with increasing x in LACO/STO. No features representative of any additional scattering due to Al/Cr inhomogeneity are observed in the XPS VB spectra. Insignificant change in the binding energy position of Cr $3d$ derived states with varying x infers that the corresponding states are more or less localized.

To identify the distribution of Ti $3d$ states in the valence band spectra, UV photons of energy of 21.2 eV are used, providing much better energy resolution and higher photoionization cross section in comparison to XPS [47]. Figure 6(b) provides the change in spectral weight in the

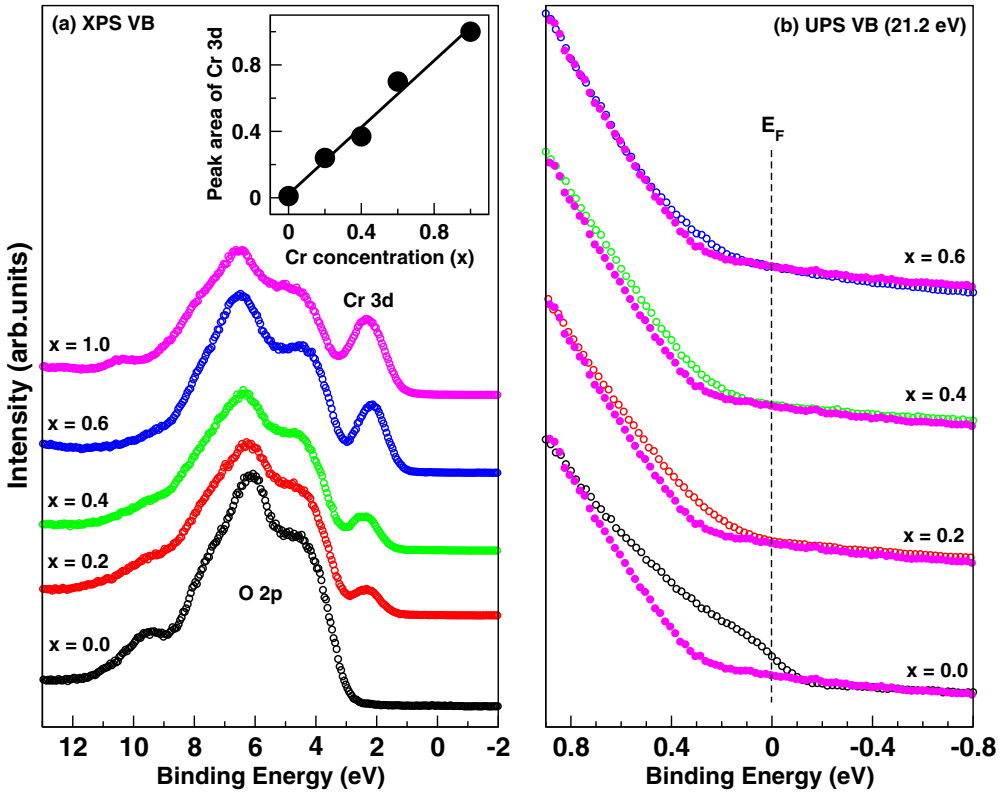

FIG. 6. (Color online) (a) XPS valence-band spectra of the $LaAl_{1-x}Cr_xO_3/SrTiO_3$ ($0 \leqslant x \leqslant 1$). Inset shows x dependence of the area of the Cr 3d derived peak. (b) Near the E_F region UPS (He I) VB spectra of the $LaAl_{1-x}Cr_xO_3/SrTiO_3$ ($0 \leqslant x \leqslant 1$) samples (open circles) are overlapped with spectrum for $x = 1$ (filled circles, magenta) to track the evolution of electronic states near E_F. The dashed line through energy zero refers to E_F.

vicinity of E_F where the UPS VB spectra corresponding to each composition have been plotted together with that of $x = 1$ (filled circles). Consistent with the earlier reports, a weak feature at the E_F related to Ti^{3+} derived states is observed for conducting the LAO/STO ($x = 0$) interface [3,33,48]. The near E_F spectral weight is found to be gradually decreasing with increasing x and an insulating gap opens up. Since we find that the Cr 3d and Ti 3d states are separated in energy by 2.4 eV, and given that Cr 3d states are localized, there exists the least possibility of charge transfer between these states in LACO/STO, contradicting the views of Chambers *et al.* [20,38]. It is evident from Fig. 6(b) that Ti^{3+} spectral weight is largest for the highest conducting sample $x = 0$, which steadily decreases with increasing x. The systematic reduction in the spectral weight of Ti^{3+} for $0 \leqslant x \leqslant 0.4$ is also reflected in the resistivity data. On the other hand, the insulating interfaces for $x \geqslant 0.6$ are manifested by an energy gap opening.

IV. DISCUSSION

Various factors, both extrinsic and intrinsic, have been associated with the origin of q-2DEG at the heterointerface of LAO/STO, $LaTiO_3$/STO, and other similar systems. Studies of heterosystems synthesized under different O_2 partial pressures, substrate temperature, and annealing temperatures [2,3,49–51] revealed that O_2 vacancies play a significant role in the q-2DEG characteristics. For a pressure variation in the range 10^{-2} to 10^{-6} mbar, the LAO/STO heterointerface still exhibits metallicity, however, with a order of magnitude change in the sheet resistance. In this context, with the growth and synthesis procedures kept similar for the deposition of LACO on TiO_2 terminated STO, the role of O_2 vacancies determining the metal-insulator transition as a function of increasing Cr concentration in the overlayer films seldom applies as a relevant factor.

The possibility of defects and that of O_2 vacancies generated at the heterointerface is partly associated with the impact of high energy species incident on the substrate. In case of energetic La ions impinging on the STO surface, cation intermixing at the heterointerface also become equally well probable [49]. As mentioned above, if cation intermixing of Sr and La drives in heterointerface q-2DEG then any La based or A-site trivalent ABO_3 type perovskite grown epitaxially on STO substrate would suffice to drive in conductivity. However, the case is not true for $LaMnO_3$ [52,53], $LaCrO_3$ [20,32,38], and $EuAlO_3$ [54] overlayer films on TiO_2 terminated STO. Instead, these heterosystems remain insulating. To address the problem in LCO/STO heterostructures, Chambers *et al.* argued that equal fraction of La/Sr and Cr/Ti in LCO/STO would be swapped across the interface, resulting in an insulating heterointerface. Such a mechanism, if it happens, would reduce the problem to that of a heterostructure composed of two nonpolar materials where an insulating heterointerface is

expected. Of relative importance of this model would be its extension to $LaMnO_3$/STO and $LaCoO_3$/STO heterostructures [55], where an insulating interface is observed. Furthermore, to account for the q-2DEG in LAO/STO heterostructures, the model ascertains that only La/Sr intersite disorder would take place, and that of Al/Ti across the interface may be partly suppressed. If valid, then this finds a lesser extension to account for the insulating interface of $EuAlO_3$/STO heterostructures, and also to account for the conducting interfaces of $LaTiO_3$/STO [56,57] and $LaVO_3$/STO heterostructures [58]. Thus a proportionate mixing of either cations across the interface, suggesting a chemically coordinated pair-correlated disorder among the constituents of the overlayer films and that of the STO substrate, appear to be less satisfactory. Besides, no chemical inhomogeneity has been explicitly observed in structural characterizations, although the question of abrupt interfaces have been raised following cross-sectional microscopic images.

It has been also shown previously that δ doping in the oxide heterointerface with transition and rare-earth elements leads to an overall decrease in the conductivity [59–62]. For example, 0.5 at. % Mn doped AlO_2 planes of LAO films with Mn/Al disorder confined to monolayers in the vicinity of the heterointerface completely suppresses the conductivity. The suppression in conductivity has been related to the formation of multiple valence states of Mn [61]. Existence of multiple valence states has also been reported in $LaMnO_3$/STO insulating superlattices [63]. Sandwiching $EuTiO_3$ (ETO) layers between LAO and STO has also been reported [62]. In this system, the q-2DEG was observed only when the thickness of ETO layers was less than 3 u.c. The critical thickness dependence of ETO suppressing q-2DEG in the LAO/ETO/STO system is explained in terms of the polar catastrophe model, where it is argued that the Coulomb repulsion hinders the transfer of electrons to the Eu derived electronic levels.

In a different way as manifested in this work, with chemical disorder ($Al_{1-x}Cr_x$) being homogeneous throughout the film, we find a gradual suppression of q-2DEG at the heterointerface. Transport measurements indicate a decreasing level of charge carrier concentration with increasing Cr concentration in the LAO overlayers. This may reflect an increasing level of Coulomb correlation effects, as $LaCrO_3$ is a Mott-Hubbard insulator. An alternate mechanism to the gradual decrease in the conductivity would be due to the increasing propensity of Cr ions to exhibit multiple valence state, as evidenced from our photoemission data. A correspondence between the Ti^{3+} and Cr^{2+} concentration is observed with increasing Cr concentration in LACO/STO heterostructures. Absence of Ti^{3+} states for $x \geqslant 0.6$ in LACO/STO and that transport measurements finding the system to be insulating, unequivocally suggests that the origin of q-2DEG at the heterointerfaces is associated with Ti^{3+} states. Thus, the concentration of Ti^{3+} ions dictate the concentration dependent metal-insulator transition in LACO/STO heterointerfaces.

The results which we obtain are in accordance with the polar catastrophe theory [10,64–71]. In LAO/STO heterostructure, an electrostatic potential builds up due to the polar nature of LAO. Polarity compensation occurs through a transfer of 0.5 e^- from the LAO overlayers to the STO substrate. Therefore, a fraction of charge flows across the interface, thereby getting confined at interface through electronic reconstruction of Ti which results in partial occupation of an otherwise empty Ti $3d$ band of STO. The conducting interface is therefore due to the itinerant Ti $3d^1$ electrons. However, the situation is significantly modified in case of LACO due the presence of Cr, which also like Ti ions have the propensity to exhibit multiple valence states. Earlier photoemission spectroscopy measurements illustrated that Cr in $LaCrO_3$ possesses strong mixed valence character and thus can assume different charge states [41]. In this scenario, the polar catastrophe at the interface of LACO/STO can be well compensated by charge redistribution in the $Al_{1-x}Cr_xO_2$ layered planes through the multiple valence of Cr ions, i.e., Cr^{3+} and Cr^{2+}. Thus, contrary to LAO/STO heterointerface, the spontaneous upward polarization of the layer-by-layer LACO film ($0.6 \leqslant x \leqslant 1$) cancels out the build-in downward polarization stimulated from the surface which is responsible for the electronic reconstruction of Ti ions at the interface. Variation in extent of Cr^{2+} and Ti^{3+} with x (as shown in Fig. 5) in LACO/STO clearly suggests that the polar catastrophe induced electronic reconstruction of Ti is progressively suppressed as more and more Cr^{2+} is created in the $Al_{1-x}Cr_xO_2$ planes. Conductivity of LAO/STO decreases with introduction of Cr in LAO ($0 \leqslant x \leqslant 0.4$) as Cr electronic reconstruction in $Al_{1-x}Cr_xO_2$ planes starts competing with Ti^{3+} reconstruction at interface. When Cr concentration is increased, $x \geqslant 0.6$, the polar catastrophe is nullified by the creation of sufficient Cr^{2+} ions, thereby having little influence of the surface charge felt at the interfaces and rendering an insulating ground state. Our results infer that the origin of the insulating nature of the interface in LCO/STO lies in the charge redistribution in LCO films as electronic reconstruction of Cr suppresses the Ti reconstruction at interface completely.

V. SUMMARY AND CONCLUSION

In summary, high quality epitaxial 6 u.c. $LaAl_{1-x}Cr_xO_3$ ($0 \leqslant x \leqslant 1$) films have been deposited on TiO_2 terminated $SrTiO_3$ (001) substrates in which the layer-by-layer growth has been observed by an *in situ* RHEED. Transport measurements find that the system exhibits heterointerface q-2DEG properties over the Cr concentration profile ($0 \leqslant x \leqslant 0.4$) and the heterointerface becomes insulating for $x \geqslant 0.6$. With the help of photoemission studies, we find multiple valence states of both Ti and Cr ions, whereby a inverse proportionality is observed between the Ti^{3+} and Cr^{2+} ion concentration with increasing x in $LaAl_{1-x}Cr_xO_3$. The progressive increase (decrease) in the concentration of Cr^{2+} (Ti^{3+}) ions as a function of x, the steady increase in the sheet resistance, and the complete disappearance of Ti^{3+} states for $x \geqslant 0.6$, which associates Ti^{3+} as a primary factor responsible for q-2DEG, lead us to conclude that electronic reconstruction is the most important and universal mechanism in these oxide heterostructures. Although more characterizations, such as thickness dependence may have to be performed, we validate that the origin of a heterointerface q-2DEG is associated with the Ti electronic reconstruction in the STO substrate, however, for heavily doped Cr samples, the required electron count necessary to nullify the polar catastrophe instability are trapped in the $LaAl_{1-x}Cr_xO_3$ overlayers. These trapped electrons show

as Cr^{2+} ions, thereby rendering the $LaAl_{1-x}Cr_xO_3$ ($x \geqslant 0.6$) heterointerface, insulating.

ACKNOWLEDGMENTS

The authors thank R. C. Budhani for stimulating discussions and Anurag Gupta for help in transport measurements. P.K. thanks CSIR for SRF. A.D. and J.J.P. acknowledges financial assistance from the CSIR XII FYP project AQuaRIUS. A.D. also acknowledges the financial support from IFCPAR (Project No. 4704-1). P.P. and A.K.S. thank CSIR XII FYP project D-NEED and CSIR network project TAPSUN (NWP-55) for financial support.

APPENDIX A: SAMPLE PREPARATION: ULTRAHIGH VACUUM (UHV) ANNEALING

Figure 7 shows the O 1*s* core-level XPS spectra of the 6 u.c. $LaAl_{1-x}Cr_xO_3/SrTiO_3$ $0 \leqslant x \leqslant 1$ samples (as-grown and annealed). The O 1*s* spectra for all as-grown samples (thin solid lines) show two features: (i) A main peak at 530 eV which originates from oxygen in the film lattice and (ii) a higher binding energy (BE) shoulder ($\simeq$532 eV) which is attributed to (OH^-) adsorbents at film surface. A few earlier PES studies on LAO/STO heterostructured systems have unequivocally reported on the presence of this surface adsorbed feature [14,20,36]. It has been recently reported that charged surface adsorbents can affect the q-2DEG properties at the oxide heterointerfaces [33,72]. We have performed an annealing treatment for all the samples as discussed in the experimental

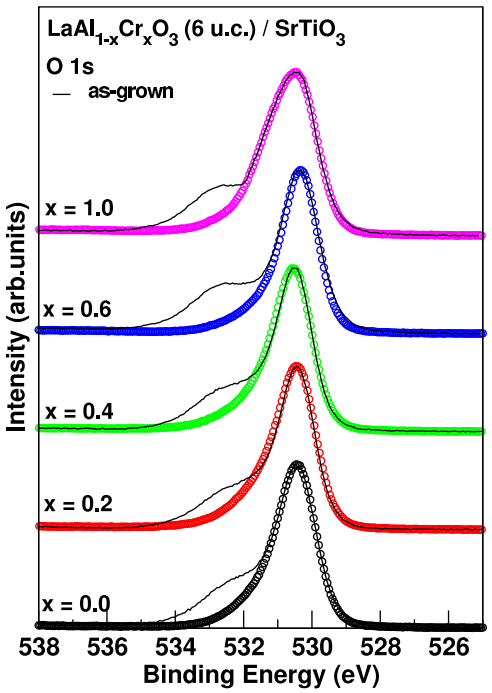

FIG. 7. (Color online) O 1*s* core-level photoemission spectra of as-loaded (thin solid lines) and *in situ* annealed (open circles) $LaAl_{1-x}Cr_xO_3$(6 u.c.)/$SrTiO_3$ samples. All the spectra have been normalized to the same peak height and shifted along the *y* axis for clarity.

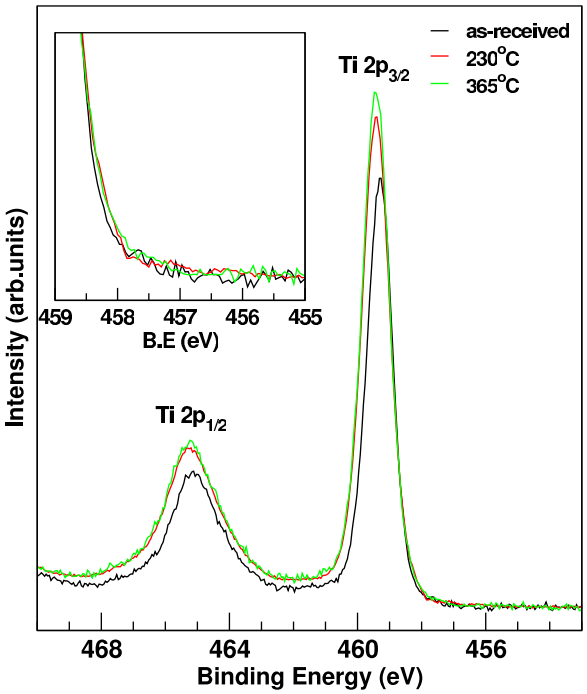

FIG. 8. (Color online) The Ti 2*p* core-level core spectra of as-received and *in situ* annealed (250 and 365 °C) TiO_2 terminated $SrTiO_3$ (001). All the spectra have been normalized at 454 eV. Inset shows close up of binding energy region where Ti^{3+} related states are expected.

section of the main text. It is evident from Fig. 1 that the feature at higher BE reduces significantly for all the samples after annealing at 350 °C. The line shape and BE position of the O 1*s* peak show negligible changes in $LaAl_{1-x}Cr_xO_3/SrTiO_3$ $0 \leqslant x \leqslant 0.4$ and small changes for $x \geqslant 0.6$.

When subjected to high temperatures ($\simeq$800 °C), it has been observed that O_2 vacancies are generated in STO [73,74] which significantly affect its electronic and transport properties [37,75,76]. For example, a change in surface conductivity at lower annealing temperatures (250−350 °C) led authors of Ref. [77] to associate the origin of surface q-2DEG in STO to the surface O_2 vacancies. On the contrary, it has also been reported that low temperature annealing of STO seldom changes the insulating nature [78,79]. Hitherto, we have performed low temperature UHV annealing so as to minimize the surface contaminants which are adsorbed on to the surface of our samples, due to its exposure to ambient conditions which occurred during the *ex situ* transfer of the samples to the UHV chamber. Our choice of 350 °C annealing in UHV not only helps in amplifying the signal to noise ratio during the PES measurements but also finds little and/or no changes in the properties of the oxide heterointerfaces. Adopting to the fact that the presence of Ti^{3+} related feature in Ti 2*p* core-level spectrum of STO would serve as an indicator to any changes in the electronic spectrum, we show in Fig. 8 the Ti 2*p* core-level spectra of the as-loaded and UHV annealed (265 and 350 °C, 6 h) TiO_2 terminated STO (001) substrates. Evidently, the inset of Fig. 8 reveal no characteristic signatures of the Ti^{3+} feature, thereby confirming the insulating nature of the post-UHV annealed STO substrates.

TABLE III. Fitting parameters for the Cr $2p_{3/2}$ core-level spectra shown in Fig. 4(b) of the main text. Binding energy (BE) positions, FWHM, relative percentage, and relative BE positions of all multiplet components and Cr^{2+} component used for fitting are given. BE position of multiplet peak is defined as ($BE_{Multiplet\ N+1} - BE_{Multiplet\ N}$), $N = 1-4$. ΔBE is BE difference between Cr^{3+} and Cr^{2+}, where the Cr^{3+} BE position is taken as the average position of dominant multiplet components 1 and 2. Relative percentage of multiplet components is calculated from the ratio of the area under individual peak and total peak area of all multiplet components. Relative percentage of Cr^{2+} is calculated from the ratio of the area under the Cr^{2+} peak and total peak area ($Cr^{2+} + Cr^{3+}$). Uncertainty in determining the BE position and FWHM is estimated to be ± 0.1 eV. Uncertainty in determining relative percentage is estimated to be $\pm 5\%$ of the base value. Our estimation of error is based on fitting of more than one experimental data set of the same sample with identical conditions, fitting using different initial guesses, and variation of fitting parameters systematically.

Sample (x)		1	0.6	0.4	0.2
Multiplet 1	BE position	576.34 ± 0.05	576.53	576.75	576.65
	FWHM	1.1 ± 0.02	1.12	1.11	1.13
	Relative %	35.6 ± 1.1	41.7	42.95	42.9
Multiplet 2	BE position	577.3 ± 0.07	577.53	577.75	577.65
	FWHM	1.1 ± 0.03	1.1	1.1	1.1
	Relative %	31.1 ± 1.2	33.7	32.5	34.5
	Relative BE position	0.96	1.0	1.0	1.0
Multiplet 3	BE position	578.1 ± 0.04	578.43	578.51	578.47
	FWHM	1.1 ± 0.03	1.1	1.1	1.1
	Relative %	15.2 ± 0.6	11.8	11.4	9.6
	Relative BE position	0.8	0.8	0.8	0.8
Multiplet 4	BE position	579.0 ± 0.09	579.33	579.41	579.37
	FWHM	1.1 ± 0.04	1.1	1.1	1.1
	Relative %	6.2 ± 0.28	5.1	5.5	6.2
	Relative BE position	0.9	0.9	0.9	0.9
Multiplet 5	BE position	579.8 ± 0.08	580.13	580.21	580.53
	FWHM	1.1 ± 0.04	1.1	1.1	1.1
	Relative %	1.8 ± 0.1	1.2	2.1	1.5
	Relative BE position	0.8	0.8	0.8	0.8
Cr^{2+} component	BE position	575.53 ± 0.1	575.63	575.84	575.73
	FWHM	2.4 ± 0.1	2.38	2.33	2.24
	Relative %	9.2 ± 0.46	7.8	5.3	5.3
	ΔBE	1.3	1.40	1.41	1.42

APPENDIX B: SUMMARY OF FITTING PARAMETERS FOR Cr $2p_{3/2}$ FITTING

All the fitting parameters (the FWHM, peak position, area, and line shape) were individually optimized for each multiplet component of Cr^{3+} and that of Cr^{2+} component, for $x = 1$ (Table III). Once optimized, the parameters were transferred to the remaining cases of $x = 0.6$, 0.4, and 0.2, keeping the relative energy separation of multiplets and their FWHM fixed, yielding a better consistency to the fit. A small change ($\pm 5\%$ of base value) in peak area was found when the FWHM or the relative energy separation were varied, with other parameters kept invariant. However, the area of each component was allowed to vary for best fitting as we noticed subtle relative change in the Cr $2p_{3/2}$ relative intensity for different x. The relative changes in the Cr $2p_{3/2}$ split peak for various Cr containing compounds could be found in Refs. [40,42,80–82]. Such changes in relative intensities has been related to various possible factors like local magnetic moment of the Cr ion [82,83], change in core hole screening [80,81], variation in $2p$-$3d$ exchange coupling [83], and configuration interaction matrix element [43].

[1] A. Ohtomo and H. Y. Hwang, Nature (London) **427**, 423 (2004).

[2] A. Kalabukhov, R. Gunnarsson, J. Börjesson, E. Olsson, T. Claeson, and D. Winkler, Phys. Rev. B **75**, 121404(R) (2007).

[3] W. Siemons, G. Koster, H. Yamamoto, W. A. Harrison, G. Lucovsky, T. H. Geballe, D. H. A. Blank, and M. R. Beasley, Phys. Rev. Lett. **98**, 196802 (2007).

[4] Y. Chen, N. Pryds, J. E. Kleibeuker, G. Koster, J. Sun, E. Stamate, B. Shen, G. Rijnders, and S. Linderoth, Nano Lett. **11**, 3774 (2011).

[5] P. R. Willmott, S. A. Pauli, R. Herger, C. M. Schlepütz, D. Martoccia, B. D. Patterson, B. Delley, R. Clarke, D. Kumah, C. Cionca, and Y. Yacobyet, Phys. Rev. Lett. **99**, 155502 (2007).

[6] A. S. Kalabukhov, Yu. A. Boikov, I. T. Serenkov, V. I. Sakharov, V. N. Popok, R. Gunnarsson, J. Börjesson, N. Ljustina, E. Olsson, D. Winkler, and T. Claeson, Phys. Rev. Lett. **103**, 146101 (2009).

[7] L. Qiao, T. C. Droubay, V. Shutthanandan, Z. Zhu, P. V. Sushko, and S. A. Chambers, J. Phys. Condens. Matter **22**, 312201 (2010).

[8] M. Gu, J. Wang, X. S. Wu, and G. P. Zhang, J. Phys. Chem. C **116**, 24993 (2012).

[9] J. J. Pulikkotil, S. Auluck, P. Kumar, A. Dogra, and R. C. Budhani, Appl. Phys. Lett. **99**, 081915 (2011).

[10] N. Nakagawa, H. Y. Hwang, and D. A. Muller, Nat. Mater. **5**, 204 (2006).

[11] S. Thiel, G. Hammerl, A. Schmehl, C. W. Schneider, and J. Mannhart, Science **313**, 1942 (2006).

[12] R. Pentcheva and W. E. Pickett, Phys. Rev. Lett. **102**, 107602 (2009).

[13] M. Sing, G. Berner, K. Goß, A. Müller, A. Ruff, A. Wetscherek, S. Thiel, J. Mannhart, S. A. Pauli, C. W. Schneider, P. R. Willmott, M. Gorgoi, F. Schäfers, and R. Claessen, Phys. Rev. Lett. **102**, 176805 (2009).

[14] A. Koitzsch, J. Ocker, M. Knupfer, M. C. Dekker, K. Dörr, B. Büchner, and P. Hoffmann, Phys. Rev. B **84**, 245121 (2011).

[15] G. Drera, F. Banfi, F. Federici Canova, P. Borghetti, L. Sangaletti, F. Bondino, E. Magnano, J. Huijben, M. Huijben, G. Rijnders, D. H. A. Blank, H. Hilgenkamp, and A. Brinkman, Appl. Phys. Lett. **98**, 052907 (2011).

[16] Y. Ishida, R. Eguchi, M. Matsunami, K. Horiba, M. Taguchi, A. Chainani, Y. Senba, H. Ohashi, H. Ohta, and S. Shin, Phys. Rev. Lett. **100**, 056401 (2008).

[17] Z. Ristic, R. Di Capua, F. Chiarella, G. M. De Luca, I. Maggio-Aprile, M. Radovic, and M. Salluzzo, Phys. Rev. B **86**, 045127 (2012).

[18] F. D. M. Haldane and P. W. Anderson, Phys. Rev. B **13**, 2553 (1976).

[19] B. R. K. Nanda and S. Satpathy, Phys. Rev. B **83**, 195114 (2011).

[20] S. A. Chambers, M. H. Engelhard, V. Shutthanandan, Z. Zhu, T. C. Droubay, L. Qiao, P. V. Sushko, T. Feng, H. D. Lee, T. Gustafsson, E. Garfunkel, A. B. Shah, J.-M. Zuo, and Q. M. Ramasseet, Surf. Sci. Rep. **65**, 317 (2010).

[21] M. L. Reinle-Schmitt, C. Cancellieri, D. Li, D. Fontaine, M. Medarde, E. Pomjakushina, C. W. Schneider, S. Gariglio, Ph. Ghosez, J.-M. Triscone and P. R. Willmott, Nat. Commun **3**, 932 (2012).

[22] M. P. Warusawithana, C. Richter, J. A. Mundy, P. Roy, J. Ludwig, S. Paetel, T. Heeg, A. A. Pawlicki, L. F. Kourkoutis, M. Zheng, M. Lee, B. Mulcahy, W. Zander, Y. Zhu, J. Schubert, J. N. Eckstein, D. A. Muller, C. Stephen Hellberg, J. Mannhart and D. G. Schlom, Nat. Commun **4**, 2351 (2013).

[23] E. Breckenfeld, N. Bronn, J. Karthik, A. R. Damodaran, S. Lee, N. Mason, and L. W. Martin, Phys. Rev. Lett. **110**, 196804 (2013).

[24] L. Qiao, T. C. Droubay, T. Varga, M. E. Bowden, V. Shutthanandan, Z. Zhu, T. C. Kaspar, and S. A. Chambers, Phys. Rev. B **83**, 085408 (2011).

[25] M. Huijben, G. Rijnders, D. Blank, S. Bals, S. Van Aert, J. Verbeeck, G. Van Tendeloo, A. Brinkman, and H. Hilgenkamp, Nat. Mater. **5**, 556 (2006).

[26] C. Bell, S. Harashima, Y. Hikita, and H. Y. Hwang, Appl. Phys. Lett. **94**, 222111 (2009).

[27] A. Savoia, D. Paparo, P. Perna, Z. Ristic, M. Salluzzo, F. M. Granozio, U. Scotti di Uccio, C. Richter, S. Thiel, J. Mannhart, and L. Marrucci, Phys. Rev. B **80**, 075110 (2009).

[28] A. Rubano, M. Fiebig, D. Paparo, A. Marino, D. Maccariello, U. Scotti di Uccio, F. M. Granozio, L. Marrucci, C. Richter, S. Paetel, and J. Mannhart, Phys. Rev. B **83**, 155405 (2011).

[29] Y. Segal, J. H. Ngai, J. W. Reiner, F. J. Walker, and C. H. Ahn, Phys. Rev. B **80**, 241107 (2009).

[30] M. Basletic, J. L. Maurice, C. Carretero, G. Herranz, O. Copie, M. Bibes, E. Jacquet, K. Bouzehouane, S. Fusil, and A. Barthelemy, Nat. Mater. **7**, 621 (2008).

[31] T. Fix, F. Schoofs, J. L. MacManus-Driscoll, and M. G. Blamire, Phys. Rev. Lett. **103**, 166802 (2009).

[32] R. Colby, L. Qiao, K. H. L. Zhang, V. Shutthanandan, J. Ciston, B. Kabius, and S. A. Chambers, Phys. Rev. B **88**, 155325 (2013).

[33] M. Takizawa, S. Tsuda, T. Susaki, H. Y. Hwang, and A. Fujimori, Phys. Rev. B **84**, 245124 (2011).

[34] C. Cancellieri, M. L. Reinle-Schmitt, M. Kobayashi, V. N. Strocov, T. Schmitt, P. R. Willmott, S. Gariglio, and J. M. Triscone, Phys. Rev. Lett. **110**, 137601 (2013).

[35] E. Slooten, Z. Zhong, H. J. A. Molegraaf, P. D. Eerkes, S. de Jong, F. Massee, E. van Heumen, M. K. Kruize, S. Wenderich, J. E. Kleibeuker, M. Gorgoi, H. Hilgenkamp, A. Brinkman, M. Huijben, G. Rijnders, D. H. A. Blank, G. Koster, P. J. Kelly, and M. S. Golden, Phys. Rev. B **87**, 085128 (2013).

[36] G. Drera, G. Salvinelli, A. Brinkman, M. Huijben, G. Koster, H. Hilgenkamp, G. Rijnders, D. Visentin, and L. Sangaletti, Phys. Rev. B **87**, 075435 (2013).

[37] P. Pal, P. Kumar, V. Aswin, A. Dogra, and A. G. Joshi, J. Appl. Phys. **116**, 053704 (2014).

[38] S. A. Chambers, L. Qiao, T. C. Droubay, T. C. Kaspar, B. W. Arey, and P. V. Sushko, Phys. Rev. Lett. **107**, 206802 (2011).

[39] L. Qiao, K. H. L. Zhang, M. E. Bowden, T. Varga, V. Shutthanandan, R. Colby, Y. Du, B. Kabius, P. V. Sushko, M. D. Biegalski, and S. A. Chambers, Adv. Funct. Mater. **23**, 2953 (2013).

[40] L. Qiao, H. Y. Xiao, S. M. Heald, M. E. Bowden, T. Varga, G. J. Exarhos, M. D. Biegalski, I. N. Ivanov, W. J. Weber, T. C. Droubay, and S. A. Chambers, J. Mater. Chem. C **1**, 4527 (2013).

[41] K. Maiti and D. D. Sarma, Phys. Rev. B **54**, 7816 (1996).

[42] M. C. Biesinger, C. Brown, J. R. Mycroft, R. D. Davidson, and N. S. McIntyre, Surf. Interface Anal. **36**, 1550 (2004).

[43] R. P. Gupta and S. K. Sen, Phys. Rev. B **12**, 15 (1975).

[44] R. P. Gupta and S. K. Sen, Phys. Rev. B **10**, 71 (1974).

[45] S. S. Li and Y. M. Hu, J. Phys. Conf. Ser. **266**, 012018 (2011).

[46] C. J. Lan, J. S. Tsay, C. K. Lo, C. A. Lin, J. H. He, and R. J. Chung, J. Electrochem. Soc. **157**, D559 (2010).

[47] J. J. Yeh and I. Lindau, At. Data Nuclear Data Tables **32**, 1 (1985).

[48] W. Siemons, G. Koster, H. Yamamoto, T. H. Geballe, D. H. A. Blank, and M. R. Beasley, Phys. Rev. B **76**, 155111 (2007).

[49] M. Huijben, A. Brinkman, G. Koster, G. Rijnders, H. Hilgenkamp, and D. H. A. Blank, Adv. Mater. **21**, 1665 (2009).

[50] J.-L. Maurice, G. Herranz, C. Colliex, I. Devos, C. Carretero, A. Barthelemy, K. Bouzehouane, S. Fusil, D. Imho, E. Jacquet, F. Jomard, D. Ballutaud, and M. Basletic, Europhys. Lett. **82**, 17003 (2008).

[51] C. Aruta, S. Amoruso, R. Bruzzese, X. Wang, D. Maccariello, F. Miletto Granozio, and U. Scotti di Uccio, Appl. Phys. Lett. **97**, 252105 (2010).

[52] H. S. Kim and H. M. Christen, J. Phys. Condens. Matter **22**, 146007 (2010).

[53] W. S. Choi, Z. Marton, S. Y. Jang, S. J. Moon, B. C. Jeon, J. H. Shin, S. S. A. Seo, T. W. Noh, K. Myung-Whun, H. N. Lee, and Y. S. Lee, J. Phys. D: Appl. Phys. **42**, 165401 (2009).

[54] M. Monti, The effect of epitaxial strain and R^{3+} magnetism on the interfaces between polar perovskites and $SrTiO_3$, Ph.D. Thesis, University of Texas at Austin, 2011.
[55] V. V. Mehta, M. Liberati, F. J. Wong, R. V. Chopdekar, E. Arenholz, and Y. Suzuki, J. Appl. Phys. **105**, 07E503 (2009).
[56] J. Biscaras, N. Bergeal, S. Hurand, C. Feuillet-Palma, A. Rastogi, R. C. Budhani, M. Grilli, S. Caprara, and J. Lesueur, Nat. Mater. **12**, 542 (2013).
[57] A. Rastogi, J. J. Pulikkotil, S. Auluck, Z. Hossain, and R. C. Budhani, Phys. Rev. B **86**, 075127 (2012).
[58] C. He, T. D. Sanders, M. T. Gray, F. J. Wong, V. V. Mehta, and Y. Suzuki, Phys. Rev. B **86**, 081401(R) (2012).
[59] H. W. Jang, D. A. Felker, C. W. Bark, Y. Wang, M. K. Niranjan, C. T. Nelson, Y. Zhang, D. Su, C. M. Folkman, S. H. Baek, S. Lee, K. Janicka, Y. Zhu, X. Q. Pan, D. D. Fong, E. Y. Tsymbal, M. S. Rzchowski, and C. B. Eom, Science **331**, 886 (2011).
[60] A. Rastogi, J. J. Pulikkotil, and R. C. Budhani, Phys. Rev. B **89**, 125127 (2014).
[61] A. Rastogi, S. Tiwari, J. J. Pulikkotil, Z. Hossain, D. Kumar, and R. C. Budhani, Euro. Phys. Lett. **106**, 57002 (2014).
[62] G. M. De Luca, R. Di Capua, E. Di Gennaro, F. M. Granozio, D. Stornaiuolo, M. Salluzzo, A. Gadaleta, I. Pallecchi, and D. Marre, C. Piamonteze, M. Radovic, Z. Ristic, and S. Rusponi, Phys. Rev. B **89**, 224413 (2014).
[63] J. Garcia-Barriocanal, F. Y. Bruno, A. Rivera-Calzada, Z. Sefrioui, N. M. Nemes, M. Garcia-Hernandez, J. Rubio-Zuazo, G. R. Castro, M. Varela, S. J. Pennycook, C. Leon, and J. Santamaria, Adv. Mater. **22**, 627 (2010).
[64] N. C. Bristowe, Emilio Artacho, and P. B. Littlewood, Phys. Rev. B **80**, 045425 (2009).
[65] Z. S. Popović, S. Satpathy, and R. M. Martin, Phys. Rev. Lett. **101**, 256801 (2008).
[66] R. Pentcheva and Warren E. Pickett, J. Phys. Condens. Matter **22**, 043001 (2010).
[67] J. Lee and A. A. Demkov, Phys. Rev. B **78**, 193104 (2008).
[68] S. A. Pauli, S. J. Leake, B. Delley, M. Björck, C. W. Schneider, C. M. Schlepütz, D. Martoccia, S. Paetel, J. Mannhart, and P. R. Willmott, Phys. Rev. Lett. **106**, 036101 (2011).
[69] J. Mannhart and D. Schlom, Science **327**, 1607 (2010).
[70] N. Reyren, S. Thiel, A. D. Caviglia, L. F. Kourkoutis, G. Hammer, C. Richter, C. W. Schneider, T. Kopp, A.-S. Rüetschi, D. Jaccard, M. Gabay, D. A. Muller, J.-M. Triscone, and J. Mannhart, Science **317**, 1196 (2007).
[71] H. Y. Hwang, Y. Iwasa, M. Kawasaki, B. Keimer, N. Nagaosa, and Y. Tokura, Nat. Mater. **11**, 103 (2012).
[72] Y. Xie, Y. Hikita, C. Bell, and H. Y. Hwang, Nat. Commun. **2**, 494 (2011).
[73] T. Nishimura, A. Ikeda, H. Namba, T. Morishita, and Y. Kido, Surf. Sci. **421**, 273 (1999).
[74] Y. Haruyama, Y. Aiura, H. Bando, Y. Nishihara, and H. Kato, J. Electron. Spectrosc. Relat. Phenom. **88–91**, 695 (1998).
[75] A. Spinelli, M. A. Torija, C. Liu, C. Jan, and C. Leighton, Phys. Rev. B **81**, 155110 (2010).
[76] Z. Q. Liu, D. P. Leusink, X. Wang, W. M. Lu, K. Gopinadhan, A. Annadi, Y. L. Zhao, X. H. Huang, S. W. Zeng, Z. Huang, A. Srivastava, S. Dhar, T. Venkatesan, and Ariando, Phys. Rev. Lett. **107**, 146802 (2011).
[77] R. Di Capua, M. Radovic, G. M. De Luca, I. Maggio-Aprile, F. M. Granozio, N. C. Plumb, Z. Ristic, U. Scotti di Uccio, R. Vaglio, and M. Salluzzo, Phys. Rev. B **86**, 155425 (2012).
[78] N. C. Plumb, M. Salluzzo, E. Razzoli, M. Månsson, M. Falub, J. Krempasky, C. E. Matt, J. Chang, M. Schulte, J. Braun, H. Ebert, J. Minár, B. Delley, K.-J. Zhou, T. Schmitt, M. Shi, J. Mesot, L. Patthey, and M. Radović, Phys. Rev. Lett. **113**, 086801 (2014).
[79] K. Takeyasu, K. Fukada, M. Matsumoto, and K. Fukutani, J. Phys. Condens. Matter **25**, 162202 (2013).
[80] M. Sperlich, C. König, G. Güntherodt, A. Sekiyama, G. Funabashi, M. Tsunekawa, S. Imada, A. Shigemoto, K. Okada, A. Higashiya, M. Yabashi, K. Tamasaku, T. Ishikawa, V. Renken, T. Allmers, M. Donath, and S. Suga, Phys. Rev. B **87**, 235138 (2013).
[81] T. Yokobori, M. Okawa, K. Konishi, R. Takei, K. Katayama, S. Oozono, T. Shinmura, T. Okuda, H. Wadati, E. Sakai, K. Ono, H. Kumigashira, M. Oshima, T. Sugiyama, E. Ikenaga, N. Hamada, and T. Saitoh, Phys. Rev. B **87**, 195124 (2013).
[82] V. Tsurkan, St. Plogmann, M. Demeter, D. Hartmann, and M. Neumann, Eur. Phys. J. B **15**, 401 (2000).
[83] A. K. Shukla, P. Krüger, R. S. Dhaka, D. I. Sayago, K. Horn, and S. R. Barman, Phys. Rev. B **75**, 235419 (2007).